An investigation of using CO_2 heat pumps to charge PCM storage tank for domestic use

Yantong Li[a], Natasa Nord[b], Huibin Yin[a,*]

[a]Guangdong Provincial Key Laboratory of Distributed Energy Systems, Dongguan University of Technology, Dongguan 523808, China

[b]Department of Energy and Process Engineering, Norwegian University of Science and Technology, Trondheim NO-7491, Norway

[*]E-mail address: yinhb@dgut.edu.cn; phone: (+86) 0769-22861808

Abstract

Current investigations mainly focused on onefold phase change material (PCM) storage tank charging process, while the integration between a heat-source device and a PCM storage tank has been seldom considered. The investigation of using a carbon dioxide (CO_2) heat pump to charge PCM storage tank is unique because PCM can enhance the system efficiency due to the delay of the outlet water temperature increase of the PCM storage tank. However, a systematic investigation about this charging process is still lacking. Therefore, this study conducted the performance investigation about the system using CO_2 heat pumps to charge the PCM storage tank. The charging process was simulated by the integration of the heat pump and PCM storage tank models. The reliabilities of these models were validated by experimental data. The effects of different expansion valve opening, PCM types, and tank arrangements on the system performance were analyzed. Both air-source and water-source CO_2 heat pumps were considered. The optimal parameters were identified by maximizing the overall performance considering the balance between the charging time and system coefficient of performance. For the system using water-source CO_2 heat pump with optimal parameters, charging time and system coefficient of performance were 0.29 h, and 3.48, respectively.

Keywords: CO_2 heat pump; PCM storage tank; Charging process; Performance investigation

Nomenclature		gs	gas cooler
E	electricity energy use	h	enthalpy
EX	exergy	in	initial
M	mass	it	inlet
$\dot{m}$	mass flowrate	lt	least preferred situation
o	opening	mt	most preferred situation
Q	energy amount	ot	outlet
$\dot{Q}$	heating capacity	ov	overall performance
SR	score	pc	PCM
T	temperature	pm	pump
tt	moment	rs	released
$\dot{W}$	power	sa	starting
		sd	supplied
Abbreviations		sm	system
CO_2	carbon dioxide	st	stored
COP	coefficient of performance	t	time
PCM	phase change material	tl	total
		wt	water
Subscripts		z	evaporator
ab	ambient		
c	specific heat	*Greek symbols*	
cc	charging	β	weight factor
chp	CO_2 heat pump	δ_0	a coefficient
cp	compressor	δ_1	a coefficient
dc	discharging	δ_2	a coefficient
dg	designed	δ_3	a coefficient
en	ending	σ	time span
ex	expansion valve	η	efficiency
ey	exergy		

1. Introduction

Rapid society development intensifies the population increase and urbanization, resulting in energy crisis [1] and environmental pollutions [2]. Therefore, it is needed to develop the sustainable energy technologies for dealing with these problems. Since heat pumps can effectively collect heat from ambient environments [3], they are known as one sustainable energy technology and have been utilized in many applications including residential heating [4], desalination [5], waste heat recovery [6], and air conditioning [7]. Dongellini et al. [8] performed the performance comparison between a hybrid heat pump system and a gas boiler system. They found that the former one could save up to 22% energy use in comparison with the latter one. Wang et al. [9] concluded that in comparison with traditional air-source heat pumps, the payback period of the system applying both air-source and water-source heat pumps was 3.66 years. Vivian et al. [10] proposed a new operating strategy for the heat pump systems for both space heating and domestic hot water purposes. It was reported that the maximum peak-power reduction could reach 35% when the strategy was applied. Kosmadakis et al. [11] investigated a high-temperature heat pump utilizing the waste heat, and they found that the shortest payback period of the system could be around 3 years.

Using CO_2 as refrigerant in heat pumps can weaken the ozone depletion caused by chlorofluorocarbons and furnish high-temperature water [12]. Dai et al. [13] concluded that at the ambient temperature of -20°C the maximum coefficient of performance (COP) for the CO_2 heat pump was 2.13 when the vapor injection technique was applied. Ahsaee and Askari [14] found that the COP of the ground-source CO_2 heat pump could be improved by 16.5% when the injector was applied. Wang et al. [15] designed a novel CO_2 heat pump for satisfying both heating and cooling demands. It was concluded that the average COP of the system was 3.27. Chung et al. [16] found that the heating and cooling COP of CO_2 heat pump could be respectively improved by 7.1% and 6.8%, when the injector with optimal injection ratio was applied.

Heat pumps are usually integrated with storage tanks in various applications, which can bring significant profits including the operating expense reduction [17]. Phase change material (PCM) has high storage density [18], which contributes to its extensively utilization in various fields including thermal management [19], photovoltaic systems [20], ventilation [21], domestic hot water use [22], and free cooling systems [23], etc. One important function of PCM is to improve the thermal capacity of storage tank. Carmona et al. [24] found that the energy and exergy efficiencies could be enhanced when PCMs were applied in the tank. Pop and Balan [25] concluded that the storage tank volume could be reduced by 25% when the PCM was applied. Kozelj et al. [26] reported that the heat storage capacity could be enhanced by approximately 70% when the PCM was applied in the water tank. Huang et al. [27] investigated a solar system with PCM storage tank, and they found that the solar fraction could be increased by around 30% when the PCM storage tank replaced the pure water tank in the system.

Many scholars have performed the studies about charging PCM storage tanks. Zhao et al. [28] found that the charging time (σ_{cc}) of PCM storage tank with 90% porosity graphite foam was 41.68% of that without graphite form. Li et al. [29] reported that increasing the mass flowrate of heat transfer fluid contributed to reducing σ_{cc} of PCM storage tank. Gorzin et al. [30] concluded that σ_{cc} could be reduced by 52% when the optimal PCM was applied. Alhusseny et al. [31] found that σ_{cc} could be effectively reduced when the metal foam was added in the PCM. Sodhi and Muthukumar [32] reported that σ_{cc} could be reduced by 24.5% when the non-uniform fin distribution was used in the PCM storage tank.

It could be found from the above literature summary that seldom investigations presented the behaviour about using the CO_2 heat pump to charge the PCM storage tank. As shown in Fig. 1, current investigations mainly aim to study the heat transfer process of charging the PCM storage tank, and seldom studies considered the issue of the integration between the heat-source device and PCM storage tank. This might cause the consideration of onefold evaluation principle for the charging process, i.e., σ_{cc}. Therefore, for proper integrations, it is very meaningful to consider more evaluation principles, e.g., σ_{cc} and the system coefficient of performance (COP_{sm}). However, the systematic investigation of this issue was still lacking. As shown in Fig. 2 (a), the temperature of the CO_2 leaving the compressor is very high. To improve the heat exchange effect between the CO_2 and the water from the PCM storage tank, the temperature of the water from the PCM storage tank should be low. As shown in Fig. 2 (b), during the charging process of the PCM, the PCM will go through the solid phase, solid-liquid two phase, and liquid phase. The solid-liquid two phase of the PCM will delay the temperature increase of the outlet water of the PCM storage tank, which will improve the energy efficiency of the CO_2 heat pump. However, the mechanisms about the effects of PCM types, tank arrangements, and expansion valve opening (o_{ex}) on the system performance are still unknown.

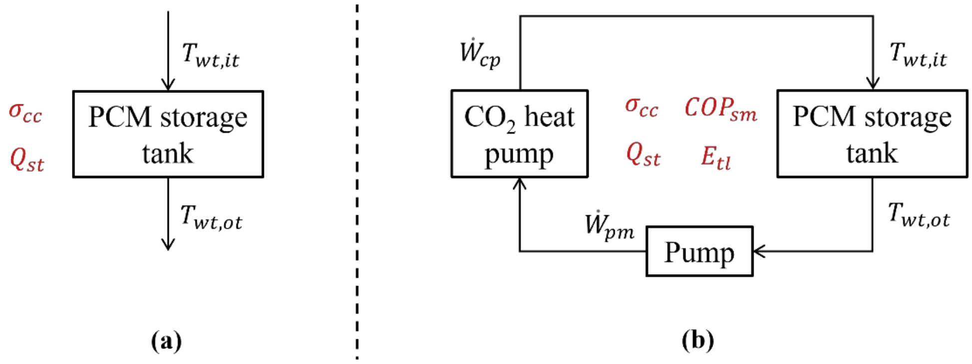

Fig. 1. Theoretical schematics of (a) current investigations and (b) this investigation

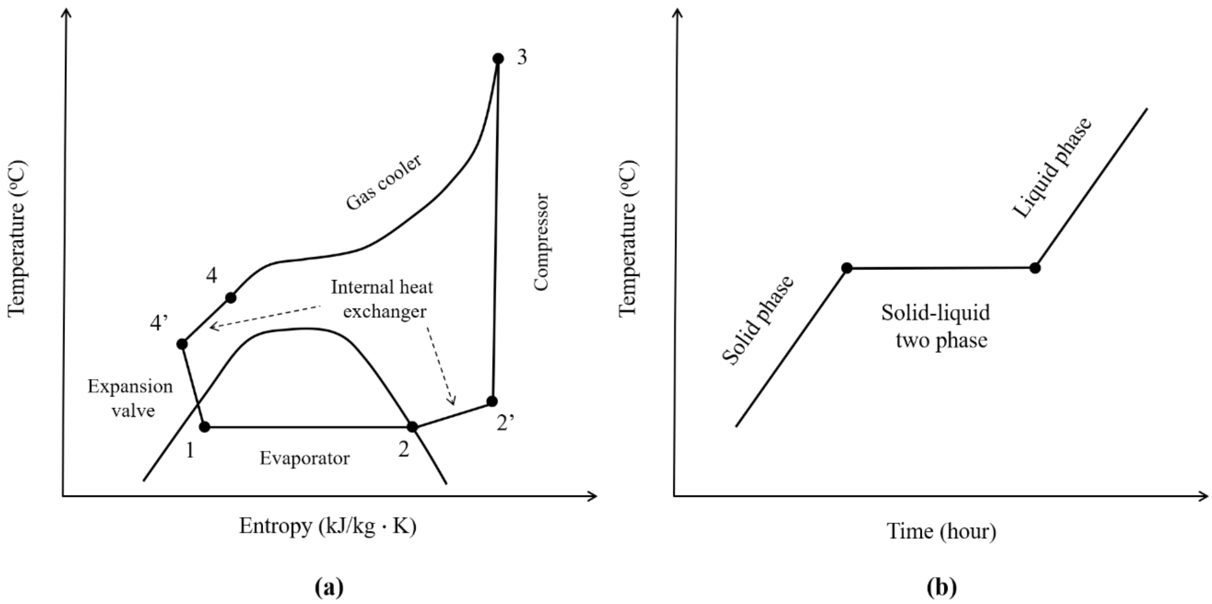

Fig. 2. (a) Temperature-entropy diagram of the refrigeration cycle in CO_2 heat pump and (b) temperature variation curve of PCM during the charging process

Hence, this study aimed to clarify the mechanisms about the effects of PCM types, tank arrangements, and o_{ex} on the system performance. This study conducted the investigation about the system of using the air-source and water-source CO_2 heat pumps to charge the PCM storage tank. The charging process was modelling by the integration of the CO_2 heat pump and PCM storage tank models. The experimental data were applied to validate the reliability of the models. The effects of different PCM types, tank arrangements, and o_{ex} on the system performance were analyzed. σ_{cc} and COP_{sm} were selected as the performance indicators. Based on the results, the multi-criterion optimization approach was performed to identify the optimal operating parameters, PCM types, and tank arrangements.

The novelties of this investigation are the followings: (a) This investigation considers the charging process integrating the heat-source device and PCM storage tank in the closed loop and thereby overcomes the limitations of traditional studies, which only considers the charging process of PCM storage tank in the open loop; (b) Two key performance indicators, i.e., charging time (σ_{cc}) and system coefficient of performance (COP_{sm}), are considered in this study. This overcomes the limitations of traditional studies which only consider σ_{cc} as the performance indicator, realizing the consideration of energy use of pumps and CO_2 heat pumps in the closed loop; (c) A multi-criterion optimization approach is established to determine the optimal o_{ex}, PCM types, and tank arrangements. This approach can well guide engineers to conduct the design for the charging system with the integration of heat-source device and PCM storage tank; (d) Both air-source and water-source CO_2 heat pumps are considered in the investigation of the charging process. These case studies play a demonstration role in the aspects of how to study the charging performance of the system integrating the advanced heat-source devices and PCM storage tank. The rest of this paper is given as the following. The methodology is introduced in Section 2. Section 3 presents the results and analysis in different expansion valve opening, PCM types, and tank arrangements. Section 4 depicts the discussion. Conclusions are given in Section 5.

2. Methodology

2.1 System description

Fig. 3 depicts the schematic for the systems of using (a) an air-source and (b) a water-source CO_2 heat pump to charge the PCM storage tank. The investigated systems were mainly comprised of the circulation pump, the expansion valve, the compressor, the liquid receiver, the evaporator, the internal heat exchanger, the gas cooler, and the PCM storage tank. The CO_2 in the evaporator will obtain heat from the mixture, composed of water and glycol for freezing protection. The CO_2 in the heat pump will go through a typical trans-critical refrigeration cycle. As shown in Fig. 2 (a), the CO_2 will evaporate in the evaporator. The CO_2 leaving the evaporator will exchange heat with that leaving the gas cooler in the internal heat exchanger. Then, CO_2 will be compressed and throttled in the compressor and expansion valve, respectively. Finally, the CO_2 will give heat to the water from the PCM storage tank in the gas cooler. The circulation pump will circulate the water between the gas cooler and the PCM storage tank. The hot water leaving the gas cooler will enter the PCM storage tank, and the cold water leaving the PCM storage tank will return the gas cooler. Normally, the charging process will be completed when the outlet water temperature of the PCM storage tank reaches the set value. This set value should be low (e.g., lower than 30°C), because the high return water temperature will reduce the COP of the CO_2 heat pump, and even cause the shutdown of the CO_2 heat pump.

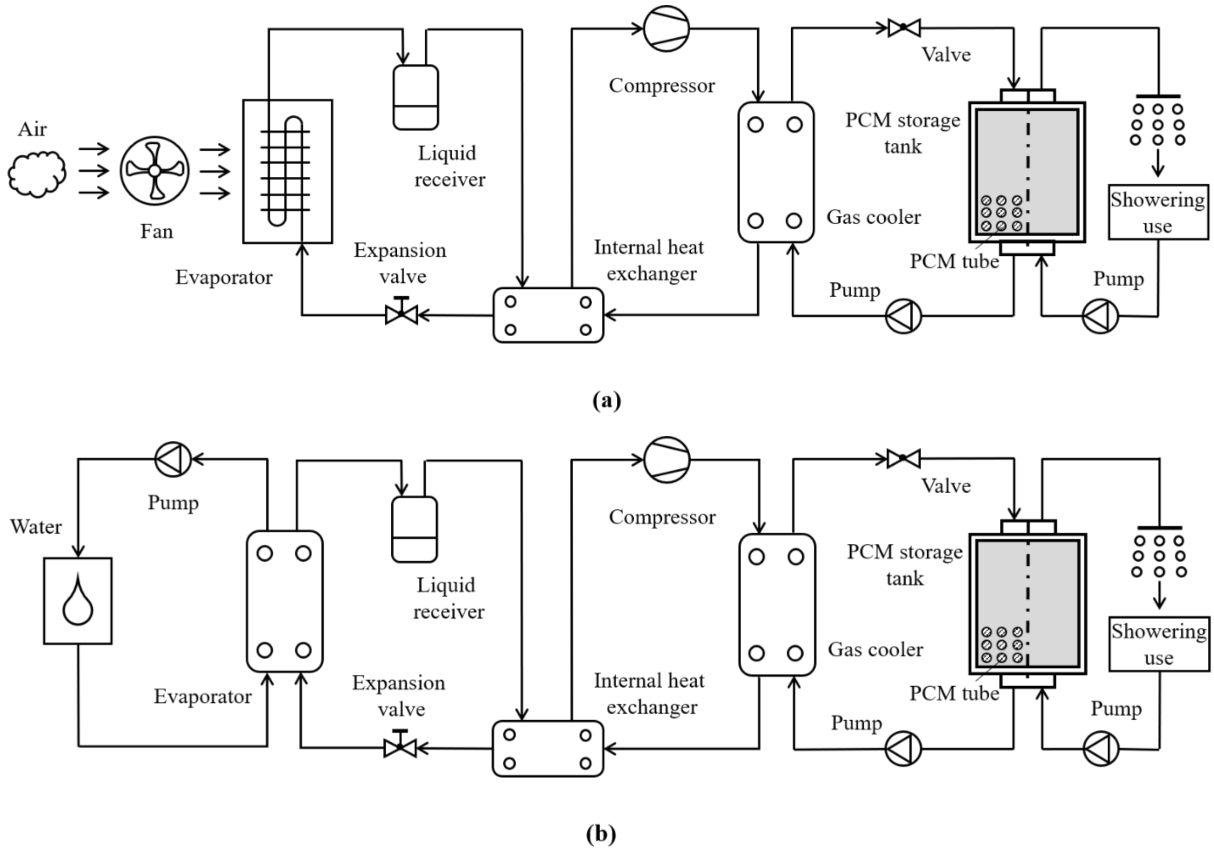

Fig. 3. Schematic for the systems of using (a) air-source and (b) water-source CO_2 heat pump to charge PCM storage tank for domestic use

2.2 System models

2.2.1 CO_2 heat pump model

The integration of MATLAB and REFPROP was applied to establish the CO_2 heat pump models. Mass and energy governing equations where several assumptions including one-dimension model without pressure drop and heat loss were applied to established the gas cooler, internal heat exchanger, and evaporator with liquid receiver models, referring to the study of Rasmussen et al. [33]. The evaporator in the air-source CO_2 heat pump was fin-tube heat exchanger. The calculations of heat transfer coefficients for the air, single-phase CO_2, and two-phase CO_2 in the fin-tube heat exchanger referred to the study of Deng et al. [34]. Expect the evaporator in the air-source heat pump, other heat exchangers in the air-source and water-source CO_2 heat pump were plate heat exchangers. The calculations of heat transfer coefficients for the single-phase and two-phase fluids referred to the study of Mota et al. [35] and Lee et al. [36]. The compressor model referred to the study of Wang et al. [37], and it was utilized to calculate the CO_2 mass flowrate through the compressor and compressor power ($\dot{W}_{cp}$). The relationships between the compressor efficiencies (i.e., volumetric, mechanical, and isentropic efficiencies) and pressure ratio that were applied in this model were constructed by the measured data in our previous study [38]. The expansion valve model referred to the study of Eames et al. [39], and it was used to calculate the CO_2 mass flowrate through the expansion valve. The relationship between the flow factor and expansion valve opening (o_{ex}) that was applied in this model was constructed by the measured data in our previous study [38].

2.2.2 PCM storage tank model

Several assumptions were applied for establishing the PCM storage tank model. The suggested model contained unchanged PCM temperature during the melting process, no heat loss to ambient, one dimensional model, and water properties that were not influenced by temperature [40]. The PCM was encapsulated inside the tubes that were install in the tank. Governing equations of the PCM storage tank model are depicted in our previous study [41]. The water and PCM Nusselt numbers were calculated referring to Watanabe et al.'s study [42].

2.3 Validation

The experimental setup for the CO_2 heat pump installed in the Energy and Indoor Environment Laboratory at the Norwegian University of Science and Technology has been established to validate the reliability of the developed CO_2 heat pump model. The detailed information of the gas cooler, evaporator, liquid receiver, internal heat exchanger, compressor, and expansion valve were presented in our previous study [43]. The accuracy of the sensors in the experimental setup were also shown in our previous study [43]. Nine cases where the discharge pressure was maintained from 7,100 kPa to 8,700 kPa with the interval of 200 kPa were conducted. The measured outlet fluid temperature in the evaporator and the gas cooler were compared with the simulated values under the same operating conditions.

The comparisons between the experimental and simulated outlet mixture temperature in the evaporator and outlet water temperature in the gas cooler in these nine cases are presented in Fig. 4. Both the simulated outlet mixture temperature in the evaporator and outlet water temperature in the gas cooler well agreed with the experimental ones. The average temperature difference between the experimental and simulated values for the outlet mixture temperature in the evaporator and outlet water temperature in the gas cooler were 2.1 K and 1.4 K, respectively. This indicated that the developed water-source CO_2 heat pump model was reliable. The reasons resulting in these temperature difference might be the measurement error of the sensors and the utilization of quasi-dynamic modelling approach. The experimental data from the literature has been compared with the simulated data of the PCM storage tank in our previous study [41]. The average relative error for the PCM storage tank model was 3.97%. The results showed that the simulated data agreed well with the experimental data, which indicated that the PCM storage tank model was reliable. Thus, the models applied to simulate the process of using CO_2 heat pump to charge the PCM storage tank were reliable.

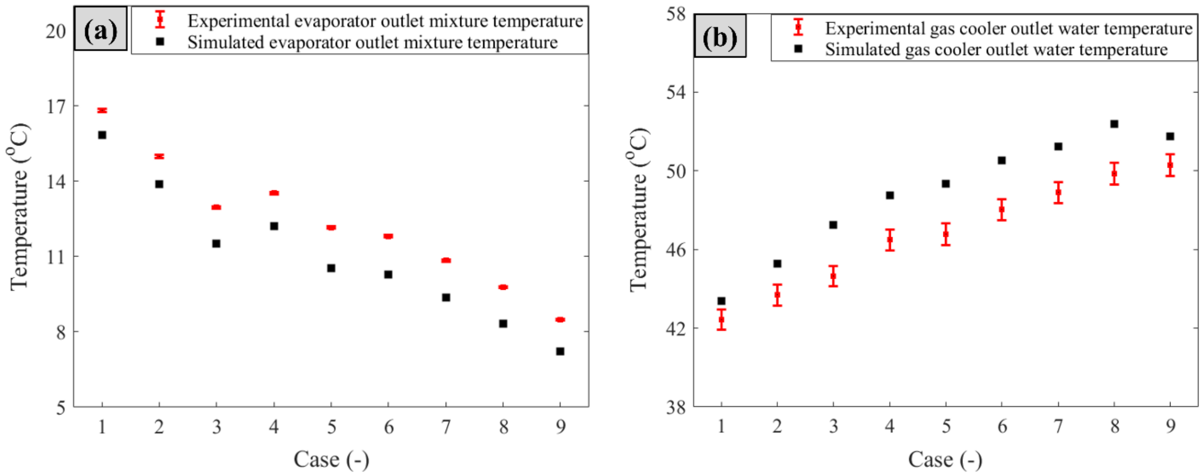

Fig. 4. Comparisons between experimental and simulated (a) outlet mixture temperature in evaporator and (b) outlet water temperature in gas cooler

2.4 Performance indicators

Two performance indicators including σ_{cc} and COP_{sm} were applied in this investigation. σ_{cc} was defined as Eqn. (1):

$$\sigma_{cc} = tt_{en} - tt_{sa} \tag{1}$$

where tt_{en} and tt_{sa} denote the ending and starting moments for charging the PCM storage tank, respectively.

COP_{sm} was defined as Eqn. (2):

$$COP_{sm} = \frac{Q_{st}}{E_{tl}} \tag{2}$$

where Q_{st} denotes the stored energy. E_{tl} denotes the total electricity energy use, which was calculated by Eqn. (3):

$$E_{tl} = E_{cp} + E_{pm,z} + E_{pm,gs} \tag{3}$$

where E_{cp}, $E_{pm,z}$, and $E_{pm,gs}$ denote the electricity energy use of compressor, pumps in the evaporator and the gas cooler, respectively. They were calculated by Eqns. (4) to (6):

$$E_{cp} = \int_{tt_{en}}^{tt_{sa}} \dot{W}_{cp}\, dt \tag{4}$$

$$E_{pm,z} = \int_{tt_{en}}^{tt_{sa}} \dot{W}_{pm,z}\, dt \tag{5}$$

$$E_{pm,gs} = \int_{tt_{en}}^{tt_{sa}} \dot{W}_{pm,gs}\, dt \tag{6}$$

where $\dot{W}_{pm,z}$ denotes the pump power in the evaporator, which was assumed to be 100 W. $\dot{W}_{pm,gs}$ denotes the pump power in the gas cooler, which was calculated by Eqn. (7):

$$\frac{\dot{W}_{pm,gs}}{\dot{W}_{pm,gs,dg}} = \delta_0 + \delta_1 \frac{\dot{m}_{gs,wt}}{\dot{m}_{gs,wt,dg}} + \delta_2 \left(\frac{\dot{m}_{gs,wt}}{\dot{m}_{gs,wt,dg}}\right)^2 + \delta_3 \left(\frac{\dot{m}_{gs,wt}}{\dot{m}_{gs,wt,dg}}\right)^3 \tag{7}$$

where dg denotes the designed value. δ_0, δ_1, δ_2, and δ_3 denote the coefficients, which were 0, 0.0016, 20.0037, and 0.9671, respectively [44]. $\dot{W}_{pm,gs,dg}$ and $\dot{m}_{gs,wt,dg}$ were 50 W and 0.044 kg/s, respectively.

The multi-criteria approach was applied to conduct the optimization for identifying the optimal parameters [3]. The score of the overall performance (SR_{ov}) was defined as Eqn. (8):

$$SR_{ov} = \beta_{\sigma_{cc}} \cdot SR_{\sigma_{cc}} + \beta_{COP_{sm}} \cdot SR_{COP_{sm}} \tag{8}$$

where SR denotes the score. β denotes the weight factor. $SR_{\sigma_{cc}}$ and $SR_{COP_{sm}}$ were respectively calculated by Eqns. (9) and (10):

$$SR_{\sigma_{cc}} = \frac{\sigma_{cc} - \sigma_{cc,lt}}{\sigma_{cc,mt} - \sigma_{cc,lt}} \tag{9}$$

$$SR_{COP_{sm}} = \frac{COP_{sm} - COP_{sm,lt}}{COP_{sm,mt} - COP_{sm,lt}} \tag{10}$$

where lt and mt denote the least-preferred and most-preferred situations, respectively. $\beta_{\sigma_{cc}}$ and $\beta_{COP_{sm}}$ were user-specified, and the relationship between them should satisfy Eqn. (11):

$$\beta_{\sigma_{cc}} + \beta_{COP_{sm}} = 1 \tag{11}$$

3. Results and analysis

The results and analysis about the influence of different expansion valve opening (o_{ex}), PCM types, and tank arrangements on the system performance are presented in this section. Charging time (σ_{cc}), stored energy (Q_{st}), total electricity energy use (E_{tl}), and system coefficient of performance (COP_{sm}) are considered as performance indicators. The optimal o_{ex}, PCM type, and tank arrangement are identified according to the results of σ_{cc} and COP_{sm}. When the identifying optimal cases according to σ_{cc} and COP_{sm} are different, the score of the overall performance (SR_{ov}) will be applied to determine the final optimal case.

3.1 Results and analysis in different expansion valve opening

This section presents the results and analyses about the effect of different expansion valve opening (o_{ex}) on the system performance. The performance indicators included charging time (σ_{cc}), stored energy (Q_{st}), total electricity energy use (E_{tl}), and system coefficient of performance (COP_{sm}). Fig. 5 depicts the variations of σ_{cc}, Q_{st}, E_{tl}, and COP_{sm} with different o_{ex} using the air-source heat pump. In Fig. 5 (a), σ_{cc} increased as o_{ex} increased. This might be caused by that lower o_{ex} resulted in higher discharge pressure and the higher CO_2 temperature to the gas cooler, leading to faster completion of charging process. When o_{ex} increased from 40% to 70%, σ_{cc} varied from 0.79 h to 2.31 h, increased by 193.1%. In Fig. 5 (b), Q_{st} increased as o_{ex} increased. Increasing o_{ex} resulted in the increase of σ_{cc}, which led to the increase of Q_{st}. When o_{ex} increased from 40% to 70%, Q_{st} varied from 3 kWh to 5.64 kWh, increased by 88.1%. In Fig. 5 (c), E_{tl} increased as o_{ex} increased. When o_{ex} increased from 40% to 70%, E_{tl} varied from 1.06 kWh to 2.83 kWh, increased by 166.9%. In Fig. 5 (d), COP_{sm} reduced as o_{ex} increased. When o_{ex} increased from 40% to 70%, COP_{sm} varied from 2.83 to 2, decreased by 29.5%. According to the Eqn. (2), this phenomenon might be explained by that the increasing degree of Q_{st} varied with o_{ex} was smaller than the increasing degree that E_{tl} varied with o_{ex}. It could be concluded that 40% was the optimal o_{ex}, because σ_{cc} in the case when o_{ex} was 40% was smaller than σ_{cc} in the other case and COP_{sm} in the case when o_{ex} was 40% was higher than COP_{sm} in the other case.

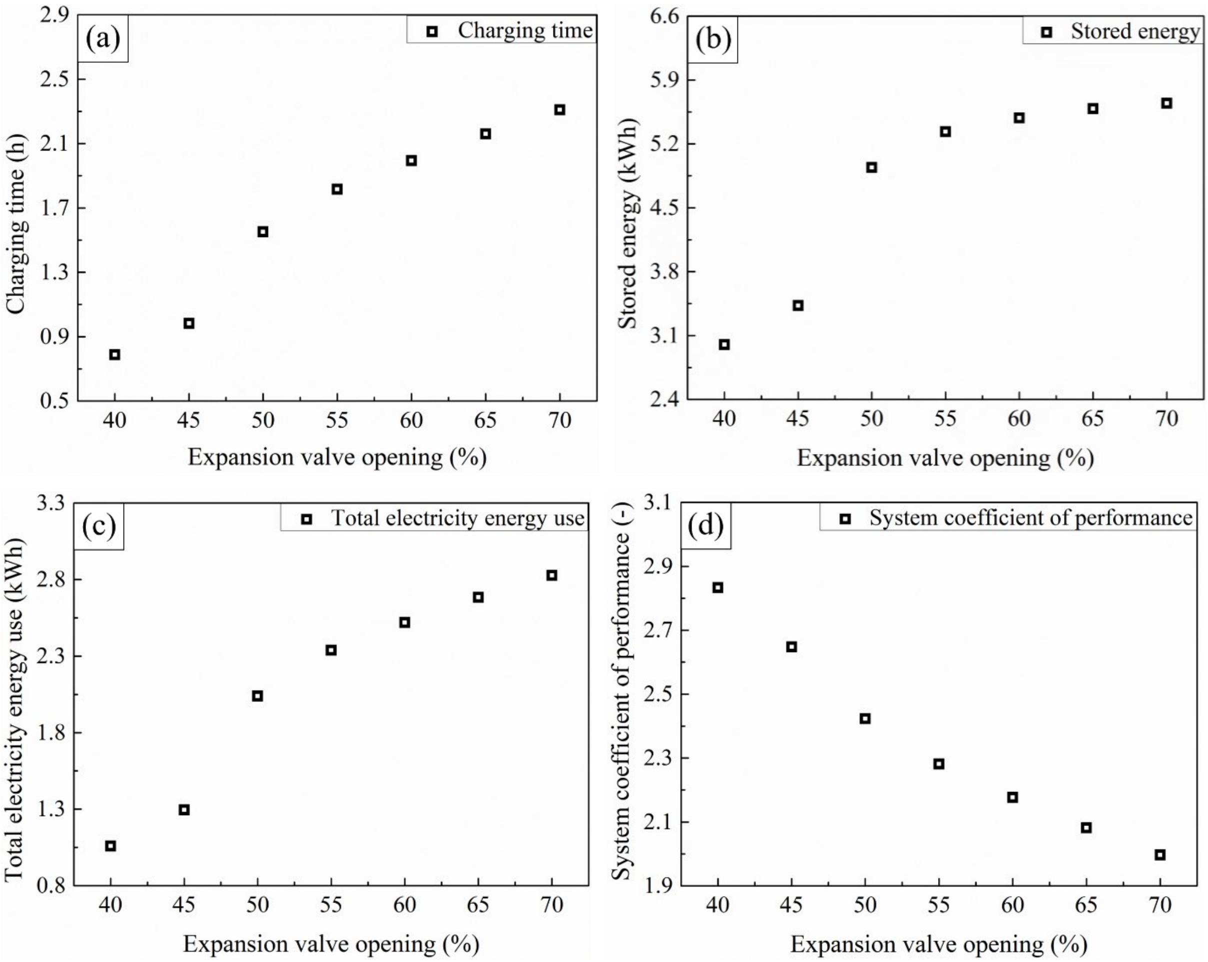

Fig. 5. Variations of (a) charging time, (b) stored energy, (c) total electricity energy use, and (d) system coefficient of performance with different expansion valve opening using the air-source heat pump

Fig. 6 depicts the variations of σ_{cc}, Q_{st}, E_{tl}, and COP_{sm} with different expansion valve opening (o_{ex}) using the water-source heat pump. In Fig. 6 (a), σ_{cc} increased as o_{ex} increased. This might be caused by that lower o_{ex} resulted in higher discharge pressure, which might increase the CO_2 temperature in the gas cooler, leading to faster completion of charging process. When o_{ex} increased from 40% to 70%, σ_{cc} varied from 0.35 h to 1.06 h, increased by 202.1%. In Fig. 6 (b), Q_{st} increased as o_{ex} increased. Increasing o_{ex} resulted in the increase of σ_{cc}, which led to the increase of Q_{st}. When o_{ex} increased from 40% to 70%, Q_{st} varied from 2.31 kWh to 3.85 kWh, increased by 67.1%. Thus, the increasing degree of σ_{cc} was higher than that of Q_{st}. In Fig. 6 (c), E_{tl} increased as o_{ex} increased. When o_{ex} increased from 40% to 70%, E_{tl} varied from 0.7 kWh to 1.38 kWh, increased by 98.3%. In Fig. 6 (d), the variations of COP_{sm} with o_{ex} was irregular. According to the Eqn. (2), this phenomenon might be explained by that in some cases the increasing degree that Q_{st} varied with o_{ex} was smaller than the increasing degree that E_{tl} varied with o_{ex}, while in some cases the increasing degree that Q_{st} varied with o_{ex} was larger than the increasing degree that E_{tl} varied with o_{ex}. The maximum COP_{sm} was 3.31, occurring at the case when o_{ex} was 40%. The minimum COP_{sm} was 2.79, occurring at the case when o_{ex} was 70%. COP_{sm} at the case when o_{ex} was 40% was 1.19 times as high as COP_{sm} at the case when o_{ex} was 70%. It could be concluded that 40% was the optimal o_{ex}, since σ_{cc} in the case when o_{ex} was 40% was smaller than σ_{cc} in the other case and COP_{sm} in the case when o_{ex} was 40% was higher than COP_{sm} in the other case.

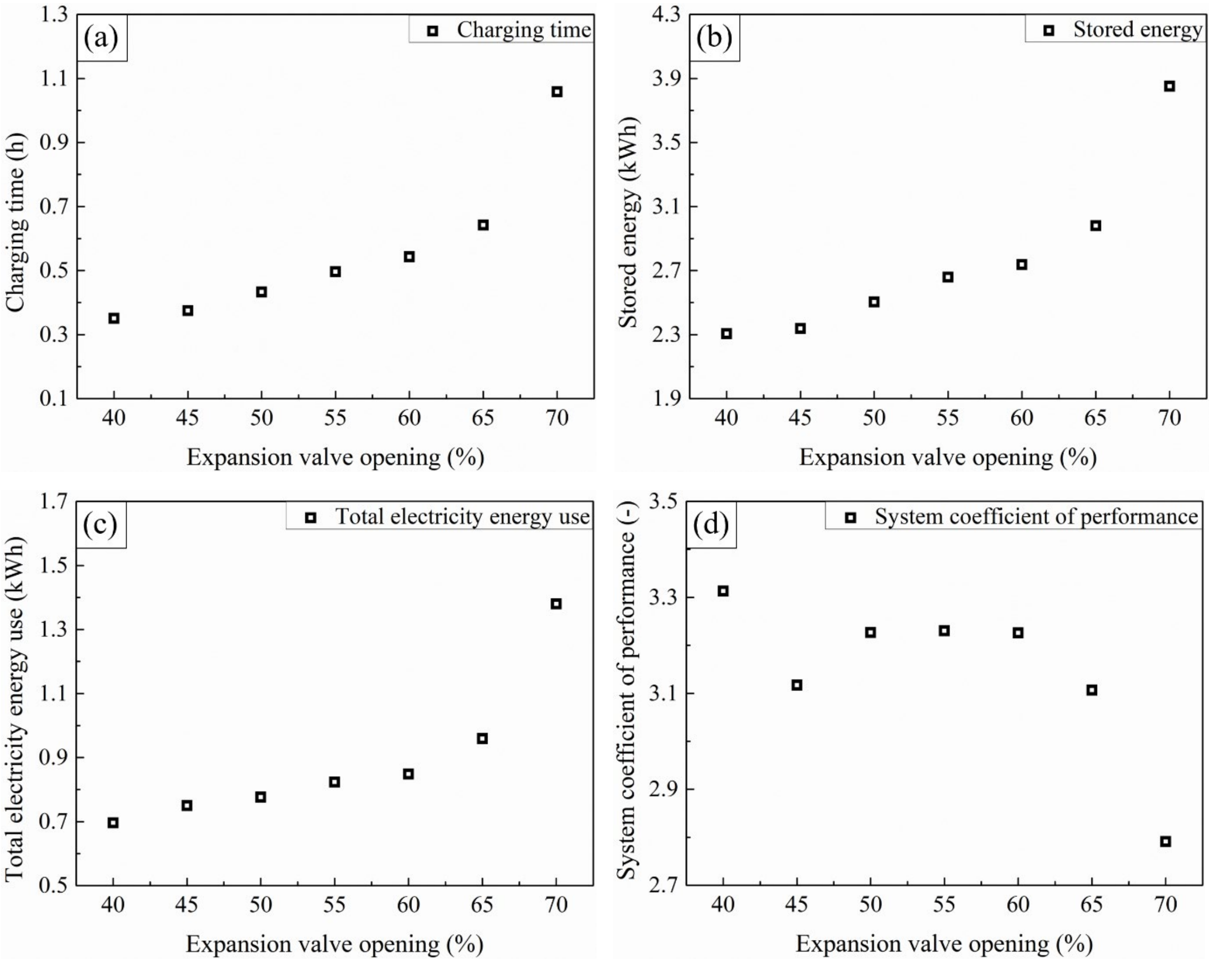

Fig. 6. Variations of (a) charging time, (b) stored energy, (c) total electricity energy use, and (d) system coefficient of performance with different expansion valve opening using the water-source heat pump

It could be seen from Fig. 5 and Fig. 6 that COP_{sm} when the water-source CO_2 heat pump was applied was higher than COP_{sm} when the air-source CO_2 heat pump was applied. The higher COP_{sm} might cause higher charging speed, which led to shorter σ_{cc}. The shorter σ_{cc} might result in less energy stored in the PCM storage tank, which meant that Q_{st} might be less. Thus, σ_{cc} when the air-source CO_2 heat pump was applied was longer than σ_{cc} when the water-source CO_2 heat pump was applied, while Q_{st} when the air-source CO_2 heat pump was applied was larger than Q_{st} when the water-source CO_2 heat pump was applied.

3.2 Results and analysis in different PCM types

This section presents the results and analysis of the system performance for different PCM types. The thermal properties of different PCM were depicted in Table 1. The PCM-1, PCM-2, PCM-3, PCM-4, PCM-5, and PCM-6 have the melting temperature of 16ºC, 17ºC, 18ºC, 19.6ºC, 20.4ºC, and 21.3ºC, respectively. The latent heat of PCM-3 that is 236 kJ/kg is the maximum, while the latent heat of PCM-4 that is 86 kJ/kg is the minimum. The solid thermal conductivity of PCM-2 that is 1 W/(m·K) is the maximum, while the solid thermal conductivity of PCM-4 that is 0.05 W/(m·K) is the minimum. The liquid thermal conductivity of PCM-2 that is 0.5 W/(m·K) is the maximum, while the liquid thermal conductivity of PCM-4 that is 0.05 W/(m·K) is the minimum. Both of the solid and liquid density of PCM-2 that are 1,800 kg/m^3 are the maximum, while both of the solid and liquid density of PCM-4 that are 694 kg/m^3 are the minimum. The solid specific heat of PCM-2 that is 2.5 kJ/(kg·K) is the maximum, while the solid specific heat of PCM-3 that is 1.65 kJ/(kg·K) is the minimum. The liquid specific heat of PCM-1 that is 2.3 kJ/(kg·K) is the maximum, while the liquid specific heat of PCM-2 that is 1.5 kJ/(kg·K) is the minimum.

Table 1 Thermal properties of different PCM

	PCM-1 [45]	PCM-2 [46]	PCM-3 [47]	PCM-4 [48]	PCM-5 [49]	PCM-6 [50]
Melting temperature (ºC)	16	17	18	19.6	20.4	21.3
Latent heat (kJ/kg)	213	145	236	86	138.8	152
Solid thermal conductivity (W/(m·K))	0.18	1	0.17	0.05	0.6	0.182
Liquid thermal conductivity (W/(m·K))	0.18	0.5	0.17	0.05	0.3	0.182
Solid density (kg/m^3)	830	1,800	780	694	881	884
Liquid density (kg/m^3)	800	1,800	780	694	881	960
Solid specific heat (kJ/(kg·K))	2.3	2.5	1.65	1.7	2	1.67
Liquid specific heat (kJ/(kg·K))	2.3	1.5	2.1	1.7	2	2.09

Fig. 7 (a) depicts the charging time (σ_{cc}) and system coefficient of performance (COP_{sm}) in different PCM types using the air-source heat pump. When the PCM-1, PCM-2, PCM-3, PCM-4, PCM-5, and PCM-6 were used, σ_{cc} were 1.56 h, 2.31 h, 0.79 h, 0.46 h, 1.25 h, and 0.61 h, respectively. Thus, σ_{cc} was the minimum when the PCM-4 was utilized, while σ_{cc} had its maximum when the PCM-2 was utilized. σ_{cc} when the PCM-2 was used was 5.02 times as high as σ_{cc} when the PCM-4 was used. These phenomena might be explained by that the density of the PCM-2 was the highest among the observed PCMs, while the density of the PCM-4 was the minimum among the PCMs. In addition, although the latent heat of the PCM-2 was lower than that of the PCM-3, the effect of the thermal capacity (i.e., multiplication of the specific heat and density) of the PCM-2 was higher than that of the PCM-3. The latent heat of the PCM-4 was evidently smaller than that of the other PCM. When the PCM-1, PCM-2, PCM-3, PCM-4, PCM-5, and PCM-6 were used, COP_{sm} were 2.7, 2.81, 2.83, 3.01, 2.76, and 2.93, respectively. Thus, COP_{sm} had its maximum when the PCM-4 was utilized, while COP_{sm} had its minimum when the PCM-1 was utilized. COP_{sm} when the PCM-4 was used was 1.11 times as high as COP_{sm} when the PCM-1 was used. It could be concluded that the PCM-4 was the optimal PCM because σ_{cc} in the case when the PCM-4 was applied was smaller than that when the other PCM was applied and COP_{sm} when the PCM-4 was applied was higher than that when the other PCM was applied.

Fig. 7 (b) depicts the stored energy (Q_{st}) and total electricity energy use (E_{tl}) for different PCM types using the air-source heat pump. When the PCM-1, PCM-2, PCM-3, PCM-4, PCM-5, and PCM-6 were used, Q_{st} were 5.69 kWh, 8.73 kWh, 3 kWh, 1.8 kWh, 4.71 kWh, and 2.35 kWh, respectively. Thus, Q_{st} was the minimum when the PCM-4 was utilized, while Q_{st} was the maximum when the PCM-2 was utilized. Q_{st} when the PCM-2 was used was 4.85 times as high as Q_{st} when the PCM-4 was used. These phenomena might be explained by the thermal properties of the PCM-4 and PCM-2 including the latent heat, density, and specific heat. When the PCM-1, PCM-2, PCM-3, PCM-4, PCM-5, and PCM-6 were used, E_{tl} were 2.11 kWh, 3.11 kWh, 1.06 kWh, 0.6 kWh, 1.7 kWh, and 0.8 kWh, respectively. Thus, E_{tl} had its minimum when the PCM-4 was utilized, while E_{tl} had its maximum when the PCM-2 was utilized. E_{tl} when the PCM-2 was used was 5.18 times as high as E_{tl} when the PCM-4 was used. This might be caused by the corresponding σ_{cc} when the different PCM were applied.

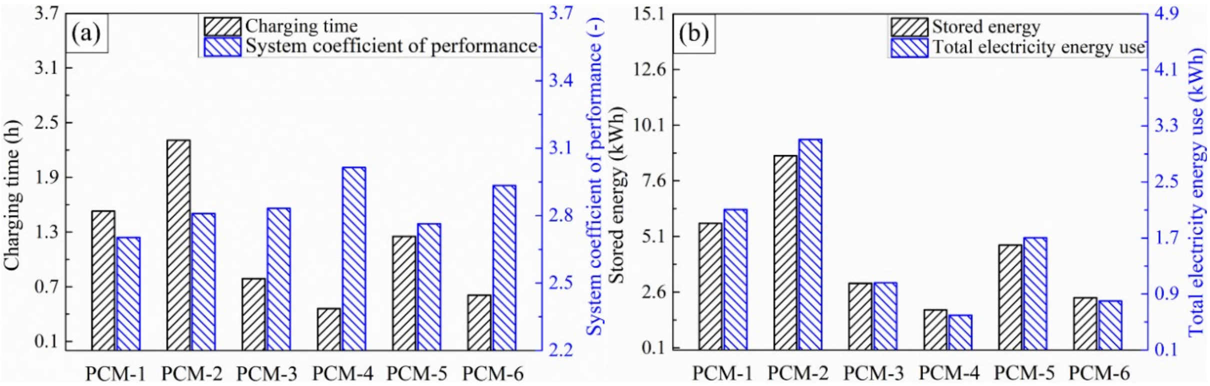

Fig. 7. (a) Charging time and system coefficient of performance, and (b) stored energy and total electricity energy use in different PCM types using the air-source heat pump

Fig. 8 (a) depicts the charging time (σ_{cc}) and system coefficient of performance (COP_{sm}) in different PCM types using the water-source heat pump. When the PCM-1, PCM-2, PCM-3, PCM-4, PCM-5, and PCM-6 were used, σ_{cc} were 0.37 h, 1.53 h, 0.35 h, 0.29 h, 0.8 h, and 0.34 h, respectively. Thus, σ_{cc} was the minimum when the PCM-4 was utilized, while σ_{cc} was the maximum when the PCM-2 was utilized. σ_{cc} when the PCM-2 was used was 5.28 times as high as σ_{cc} when the PCM-4 was used. These phenomena might be explained by that the density of the PCM-2 was the maximum among these PCM, while the density of the PCM-4 was the minimum among these PCM. When the PCM-1, PCM-2, PCM-3, PCM-4, PCM-5, and PCM-6 were used, COP_{sm} were 3.23, 2.32, 3.31, 3.48, 3.03, and 3.27, respectively. Thus, COP_{sm} was the maximum when the PCM-4 was utilized, while COP_{sm} was the minimum when the PCM-2 was utilized. COP_{sm} when the PCM-4 was used was 1.5 times as high as COP_{sm} when the PCM-2 was used. It could be concluded that the PCM-4 was the optimal PCM since σ_{cc} in the case when the PCM-4 was applied was smaller than that when the other PCM was applied and COP_{sm} in the case when the PCM-4 was applied was larger than that when the other PCM was applied.

Fig. 8 (b) depicts the stored energy (Q_{st}) and total electricity energy use (E_{tl}) in different PCM types using the air-source heat pump. When the PCM-1, PCM-2, PCM-3, PCM-4, PCM-5, and PCM-6 were used, Q_{st} were 2.41 kWh, 8.7 kWh, 2.31 kWh, 1.98 kWh, 4.5 kWh, and 2.28 kWh, respectively. Thus, Q_{st} had its minimum when the PCM-4 was utilized, while Q_{st} was the maximum when the PCM-2 was utilized. Q_{st} when the PCM-2 was used was 4.39 times as high as Q_{st} when the PCM-4 was used. These might be caused by the thermal properties of the PCM-4 and PCM-2. When the PCM-1, PCM-2, PCM-3, PCM-4, PCM-5, and PCM-6 were used, E_{tl} were 0.75 kWh, 3.74 kWh, 0.7 kWh, 0.57 kWh, 1.49 kWh, and 0.7 kWh, respectively. Thus, E_{tl} had its minimum when the PCM-4 was utilized, while E_{tl} had its maximum when the PCM-2 was utilized. E_{tl} when the PCM-2 was used was 6.56 times as high as E_{tl} when the PCM-4 was used. This might be caused by the corresponding σ_{cc} when the different PCM were applied.

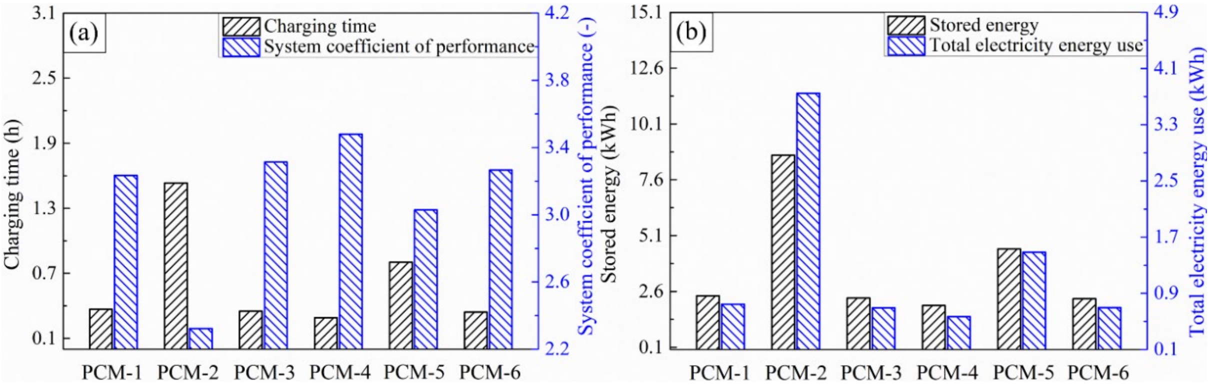

Fig. 8. (a) Charging time and system coefficient of performance, and (b) stored energy and total electricity energy use in different PCM types using the water-source heat pump

For the system using the air-source and water-source CO_2 heat pumps, the optimal PCM type was PCM-4. When the PCM-4 was applied in the systems using air-source or water-source CO_2 heat pumps, σ_{cc} had its minimum, and COP_{sm} had its maximum. The good thermal properties of PCM-4 led to be that it could contribute to realizing the charging process within a shorter period and better energy performance.

3.3 Results and analysis in different tank arrangements

This section presents the results and analysis of the system performance in different tank arrangements. PCM-4 was applied in this section. The number of tubes in each column and row in different cases were depicted in Table 2. The number of tubes in each column in Case 1, Case 2, Case 3, Case 4, Case 5, and Case 6 were 21, 20, 19, 21, 20, and 19, respectively. The number of tubes in each row in Case 1, Case 2, Case 3, Case 4, Case 5, and Case 6 were 6, 6, 6, 5, 5, and 5, respectively.

Table 2 Number of tubes in each column and row in different cases

	Case 1	Case 2	Case 3	Case 4	Case 5	Case 6
Number of tubes in each column (-)	21	20	19	21	20	19

Number of tubes in each row (-)	6	6	6	5	5	5

Fig. 9 (a) depicts the charging time (σ_{cc}) and system coefficient of performance (COP_{sm}) in different tank arrangements using the air-source heat pump. σ_{cc} in Case 1, Case 2, Case 3, Case 4, Case 5, and Case 6 were 0.62 h, 0.58 h, 0.55 h, 0.49 h, 0.46 h, and 0.43 h, respectively. Thus, σ_{cc} in Case 1 was the maximum, while σ_{cc} in Case 6 was the minimum. σ_{cc} in Case 1 was 1.44 times as high as σ_{cc} in Case 6. COP_{sm} in Case 1, Case 2, Case 3, Case 4, Case 5, and Case 6 were 3.011, 3.0104, 3.0099, 3.0142, 3.0141, and 3.014, respectively. The difference of COP_{sm} between different cases was very small. According to the results of σ_{cc} in different cases, the tank arrangement in Case 6 was optimal because σ_{cc} in Case 6 was smaller than that in the other case. However, according to the results of COP_{sm} in different cases, the tank arrangement in Case 4 was optimal because COP_{sm} was slightly higher than that in the other case. Thus, it was important to identify the optimal tank arrangements based on the results in Fig. 9 (a). Further analysis for identifying the optimal tank arrangements is presented in the Fig. 10.

Fig. 9 (b) depicts the stored energy (Q_{st}) and total electricity energy use (E_{tl}) in different tank arrangements using the air-source heat pump. Q_{st} in Case 1, Case 2, Case 3, Case 4, Case 5, and Case 6 were 2.41 kWh, 2.28 kWh, 2.15 kWh, 1.91 kWh, 1.8 kWh, and 1.7 kWh, respectively. Thus, Q_{st} in Case 1 had its maximum, while Q_{st} in Case 6 had its minimum. Q_{st} in Case 1 was 1.42 times as high as Q_{st} in Case 6. E_{tl} in Case 1, Case 2, Case 3, Case 4, Case 5, and Case 6 were 0.8 kWh, 0.76 kWh, 0.72 kWh, 0.63 kWh, 0.6 kWh, and 0.56 kWh, respectively. Thus, E_{tl} in Case 6 had its minimum, while E_{tl} in the Case 1 had its maximum. E_{tl} in Case 1 was 1.43 times as high as E_{tl} in Case 6. According to the structure parameters in Table 2, the volume of PCM storage tank in Case 1 and Case 6 had its maximum and minimum, respectively. Therefore, the difference of PCM storage tank volume might explain the difference of Q_{st} and E_{tl} in different tank arrangements.

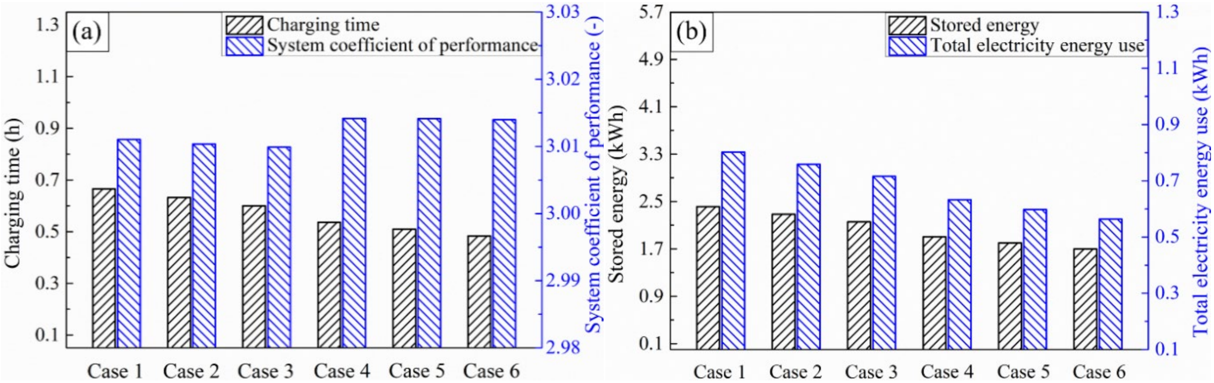

Fig. 9. (a) Charging time and system coefficient of performance, and (b) stored energy and total electricity energy use in different tank arrangements using the air-source heat pump

Fig. 10 depicts the score of the overall performance (SR_{ov}) in different tank arrangements using the air-source heat pump. PCM-4 was applied in this section. When the weight factor for σ_{cc} ($\beta_{\sigma_{cc}}$) and the weight factor for COP_{sm} ($\beta_{COP_{sm}}$) were 0.4 and 0.6, SR_{ov} in Case 1, Case 2, Case 3, Case 4, Case 5, and Case 6 were 0.16, 0.14, 0.14, 0.88, 0.94, and 0.97, respectively. Thus, the tank arrangement in the Case 6 was optimal because SR_{ov} was the highest. When $\beta_{\sigma_{cc}}$ and $\beta_{COP_{sm}}$ were 0.6 and 0.4, SR_{ov} in Case 1, Case 2, Case 3, Case 4, Case 5, and Case 6 were 0.11, 0.15, 0.22, 0.83, 0.91, and 0.98, respectively. Thus, the tank arrangement in the Case 6 was optimal because SR_{ov} was the highest. It could be seen that no matter that σ_{cc} had a higher weighting or COP_{sm} had a higher weighting, the tank arrangement in Case 6 was optimal. This meant that the balance of σ_{cc} and COP_{sm} in Case 6 could be better established than that in the other cases.

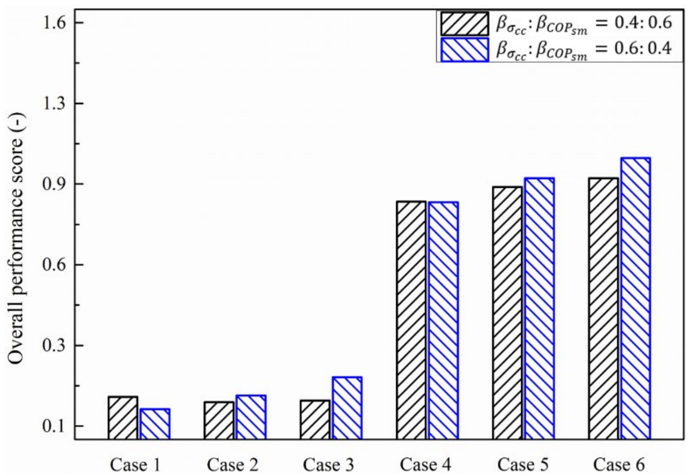

Fig. 10. Overall performance score in different tank arrangements using the air-source heat pump

Fig. 11 (a) depicted the charging time (σ_{cc}) and system coefficient of performance (COP_{sm}) in different tank arrangements using the water-source heat pump. PCM-4 was applied in this section. σ_{cc} in Case 1, Case 2, Case 3, Case 4, Case 5, and Case 6 were 0.38 h, 0.36 h, 0.33 h, 0.31 h, 0.29 h, and 0.27 h, respectively. Thus, σ_{cc} in Case 1 had its maximum, while σ_{cc} in Case 6 had its minimum. σ_{cc} in Case 1 was 1.41 times as high as σ_{cc} in Case 6. COP_{sm} in Case 1, Case 2, Case 3, Case 4, Case 5, and Case 6 were 3.4847, 3.466, 3.4704, 3.4787, 3.4793, and 3.4624, respectively. The difference of COP_{sm} among different cases was small. However, it could be still found that COP_{sm} in Case 1 was the highest, while COP_{sm} in Case 6 was the lowest. According to the results of σ_{cc} for different cases, the tank arrangement in Case 6 was optimal because σ_{cc} was smaller than that in the other case. However, according to the results of COP_{sm} in different cases, the tank arrangement in Case 1 was optimal because COP_{sm} was slightly bigger than that in the other case. Thus, it was necessary to identify the optimal tank arrangement according to the results in Fig. 11 (a). Further analysis for identifying the optimal tank arrangement is presented in Fig. 12.

Fig. 11 (b) depicts the stored energy (Q_{st}) and total electricity energy use (E_{tl}) in different tank arrangements using the water-source heat pump. Q_{st} in Case 1, Case 2, Case 3, Case 4, Case 5, and Case 6 were 2.55 kWh, 2.41 kWh, 2.27 kWh, 2.09 kWh, 1.98 kWh, and 1.86 kWh, respectively. Thus, Q_{st} in Case 1 was the maximum, while Q_{st} in Case 6 was the minimum. Q_{st} in Case 1 was 1.37 times as high as Q_{st} in Case 6. E_{tl} in Case 1, Case 2, Case 3, Case 4, Case 5, and Case 6 were 0.73 kWh, 0.7 kWh, 0.66 kWh, 0.6 kWh, 0.57 kWh, and 0.54 kWh, respectively. Thus, E_{tl} in Case 6 had its minimum, while E_{tl} in Case 1 had its maximum. E_{tl} in Case 1 was 1.35 times as high as E_{tl} in Case 6. The PCM storage tank volume in Case 1 and Case 6 were the maximum and minimum among these cases, respectively. This might be the reason why Q_{st} and E_{tl} had its maximum in Case 1, and Q_{st} and E_{tl} had its maximum in Case 6.

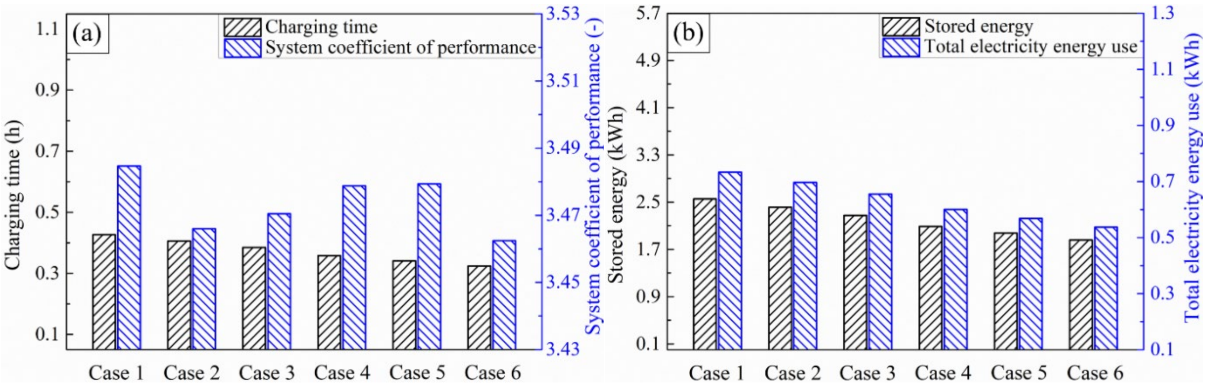

Fig. 11. (a) Charging time and system coefficient of performance, and (b) stored energy and total electricity energy use in different tank arrangements using the water-source heat pump

Fig. 12 depicts the score of the overall performance (SR_{ov}) in different tank arrangements using the water-source heat pump. PCM-4 was applied in this section. When the weight factor of σ_{cc} ($\beta_{\sigma_{cc}}$) and weight factor of COP_{sm} ($\beta_{COP_{sm}}$) were 0.4 and 0.6, SR_{ov} in Case 1, Case 2, Case 3, Case 4, Case 5, and Case 6 were 0.6, 0.18, 0.38, 0.71, 0.79, and 0.4, respectively. Thus, the tank arrangement in Case 5 was optimal because SR_{ov} was the highest. When $\beta_{\sigma_{cc}}$ and $\beta_{COP_{sm}}$ were 0.6 and 0.4, SR_{ov} in Case 1, Case 2, Case 3, Case 4, Case 5, and Case 6 were 0.4, 0.19, 0.39, 0.69, 0.8, and 0.6, respectively. Thus, the tank arrangement in Case 5 was optimal because SR_{ov} was the highest. It could be seen that no matter that σ_{cc} had a higher weighting or COP_{sm} had a higher weighting, the tank arrangement in Case 5 was optimal. This meant that the balance of σ_{cc} and COP_{sm} in Case 5 could be better established than that in the other case.

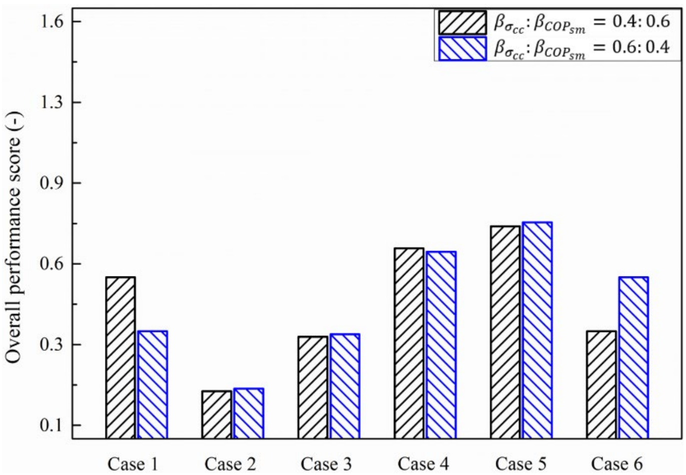

Fig. 12. Overall performance score in different tank arrangements using the water-source heat pump

For the system using the air-source and water-source CO_2 heat pumps, the optimal cases about the tank arrangements were Case 6 and Case 5, respectively. According to the Eqn. (8), the identification of optimal cases was related to σ_{cc}, COP_{sm}, $\beta_{\sigma_{cc}}$, and $\beta_{COP_{sm}}$. It might be difficult to determine the optimal tank arrangements according to the single factor. However, this section gave guidelines how to identify the optimal tank arrangements, which was significant in the engineering applications.

4. Discussion

The performance of the system utilizing the CO_2 heat pumps to charge the PCM storage tank was studied, considering charging time (σ_{cc}) and system coefficient of performance (COP_{sm}) as indicators. The effects of expansion valve opening (o_{ex}), PCM types, and tube arrangements on σ_{cc}, COP_{sm}, stored energy (Q_{st}) and total electricity energy use (E_{tl}) were analyzed. The multi-criteria optimization approach was applied to identify the optimal o_{ex}, PCM types, and tube arrangements. This study considered two kinds of CO_2 heat pumps (i.e., air-source and water-source CO_2 heat pumps) as case studies. This study broke the traditional research paths about the charging performance studies of PCM storage tank, which only studied the charging process in the open loop and applied σ_{cc} as the indicator. This study established a different research path, which considered the charging process in the closed loop, and applied both σ_{cc} and COP_{sm} as the indicators. This study not only filled the research gap of the investigations of the system applying CO_2 heat pumps to charge the PCM storage tank, but also gave a guideline for engineers to well determine optimal parameters of the system. Based on our study, the future studies on the following topics may be initiated: (a) more advanced heat-source devices (e.g., ground-source and solar-assisted CO_2 heat pumps) should be considered in the investigations for the charging performance of the PCM storage tank in the closed loop. The effects of different parameters (e.g., borehole depth in the ground-source CO_2 heat pump and solar collector area in the solar-assisted CO_2 heat pump) on the system performance should be considered; (b) different PCM types should be considered in the investigation of the charging process. A dataset of PCM types should be established and applied in different charging systems. The optimal PCM types for different charging systems could be better to be determined; (c) optimal operating strategies (e.g., artificial neural network-based and self-adaptive optimal control methods) for different charging systems should be constructed for obtaining smaller σ_{cc} and larger COP_{sm}. Our study gave a start point how to present and compare the results for different improvements and specific system adjustments.

5. Conclusions

The performance investigation of using the CO_2 heat pumps to charge the PCM storage tank was performed in this study. The modelling of the charging process was constructed by the integration of the heat pump and PCM storage tank models. Experimental data were applied for validating the reliability of these models. The influence of different expansion valve opening (o_{ex}), PCM types, and tube arrangements on the system performance were analyzed. Both the air-source and the water-source CO_2 heat pumps were considered in this study. The optimal parameters were identified by maximizing the overall performance considering the balance between the charging time (σ_{cc}) and system coefficient of performance (COP_{sm}). For the systems using both air-source and water-source CO_2 heat pumps, σ_{cc} increased with the increase of o_{ex}. The optimal o_{ex} was 40% because σ_{cc} in was the shortest and COP_{sm} was the highest. COP_{sm} in the cases when o_{ex} was 40% using the air-source and the water-source CO_2 heat pumps were 2.83 and 3.31, respectively. For the systems using both the air-source and the water-source CO_2 heat pumps, the optimal PCM was the PCM-4 with the melting temperature of 19.6°C and the latent heat of 86 kJ/kg. COP_{sm} when the PCM-4 was applied using the air-source and the water-source CO_2 heat pumps were 3.01 and 3.48, respectively. For the system using the air-source CO_2 heat pump, the optimal tank arrangement occurred at Case 6, in which the number of tubes in each column and row were 19 and 5, respectively. COP_{sm} in Case 6 when the air-source CO_2 heat pump was applied was 3.014. For the system using the water-source CO_2 heating pump, the optimal tank arrangement occurred at Case 5, in which the number of tubes in each column and row were 20 and 5, respectively. COP_{sm} in Case 5 when the water-source CO_2 heat pump was applied was 3.4793. In sum, for the systems using both air-source and water-source CO_2 heat pumps, PCM-4 was the most suitable. For the system using the air-source and water-source CO_2 heat pumps, the optimal cases about the tank arrangements were Case 6 and Case 5, respectively. The identification of optimal cases was related to σ_{cc}, COP_{sm}, $\beta_{\sigma_{cc}}$, and $\beta_{COP_{sm}}$. It might be hard to determine the optimal tank arrangement according to the single factor. However, this study could guide engineers to identify the optimal o_{ex}, PCM types, and tank arrangements, which was significant in the engineering applications.

Acknowledgements

This work is supported by Guangdong Basic and Applied Basic Research Foundation (2022A1515140105). This work is supported by Guangdong Provincial Key Laboratory of

Distributed Energy Systems, No.2020B1212060075. This project has received funding from the European Union's Horizon 2020 research and innovation programme under the Marie Skłodowska-Curie grant agreement No [895732].

Appendix A. Performance analysis of discharging process

Fig. A1 (a) depicts the discharging time (σ_{dc}) and released energy (Q_{rs}) in different PCM types. When the PCM-1, PCM-2, PCM-3, PCM-4, PCM-5, and PCM-6 were used, σ_{dc} were 1.09 h, 1.5 h, 0.86 h, 1.06 h, 0.82 h, and 0.98 h, respectively. Thus, σ_{dc} was the minimum when the PCM-5 was utilized, while σ_{dc} had its maximum when the PCM-2 was utilized. σ_{dc} when the PCM-2 was utilized was 1.83 times as high as σ_{dc} when the PCM-5 was utilized. When the PCM-1, PCM-2, PCM-3, PCM-4, PCM-5, and PCM-6 were used, Q_{rs} were 2.33 kWh, 3.2 kWh, 2.14 kWh, 1.92 kWh, 2.31 kWh, and 2.24 kWh, respectively. Thus, Q_{rs} had its maximum when the PCM-2 was utilized, while Q_{rs} had its minimum when the PCM-4 was utilized. Q_{rs} when the PCM-4 was utilized was 1.67 times as high as Q_{rs} when the PCM-2 was utilized. It could be seen that in Table 1 the density of PCM-2 was higher than that of other PCMs, and the density of PCM-4 was lower than that of other PCMs. The degree that the density of PCM-2 was higher than that of other PCMs was evident, which caused that PCM-2 has higher thermal capacity (i.e., multiplication of the specific heat and density). Meanwhile, PCM-4 has lower latent heat. Thus, thermal properties of these PCMs might explain the difference of σ_{dc} and Q_{rs} in different PCM types.

Fig. A1 (b) depicts σ_{dc} and Q_{rs} in different tank arrangements. σ_{dc} in Case 1, Case 2, Case 3, Case 4, Case 5, and Case 6 were 1.28 h, 1.23 h, 1.18 h, 1.1 h, 1.06 h, and 1.01 h, respectively. Thus, σ_{dc} in Case 1 was the maximum, while σ_{dc} in Case 6 was the minimum. σ_{dc} in Case 1 was 1.27 times as high as σ_{dc} in Case 6. Q_{rs} in Case 1, Case 2, Case 3, Case 4, Case 5, and Case 6 were 2.45 kWh, 2.33 kWh, 2.21 kWh, 2.02 kWh, 1.92 kWh, and 1.82 kWh, respectively. Thus, Q_{rs} in Case 1 had its maximum, while Q_{rs} in Case 6 had its minimum. Q_{rs} in Case 1 was 1.35 times as high as Q_{rs} in Case 6. According to the structure parameters in Table 2, the volume of PCM storage tank in Case 1 had its maximum, while the volume of PCM storage tank in Case 6 had its minimum. Thus, the difference of PCM storage tank volume might explain the difference of σ_{dc} and Q_{rs} in different tank arrangements.

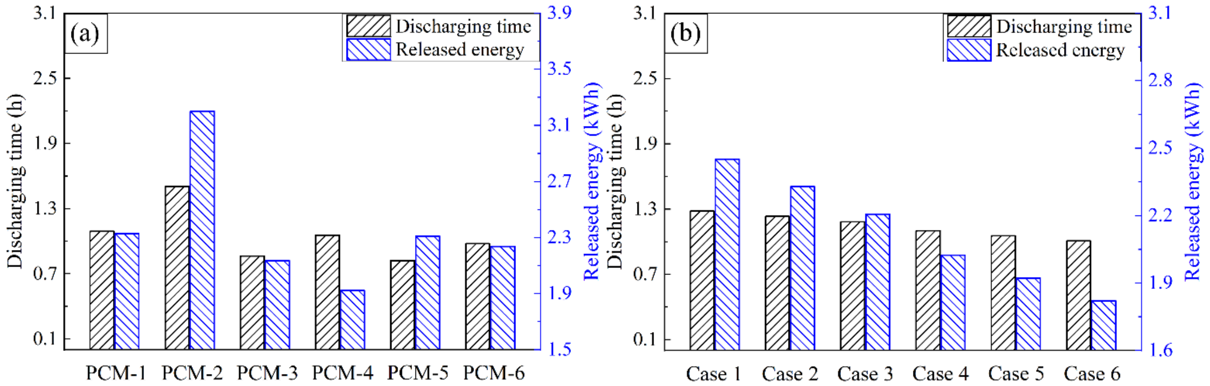

Fig. A1. Discharging time and released energy in different (a) PCM types and (b) tank arrangements

Appendix B. Effect of ambient temperature on performance of CO_2 heat pump

Fig. B1 (a) depicts the variations of heating capacity ($\dot{Q}_{gs}$), compressor power ($\dot{W}_{cp}$), and coefficient of performance of CO_2 heat pump (COP_{chp}) with different ambient air temperature (T_{ab}) using the air-source heat pump. $\dot{Q}_{gs}$ increased with the increase of T_{ab}. This might be caused by that the increase of T_{ab} led to the increasing temperature difference between the ambient air and CO_2 in the evaporator, which improved the heat transfer effect. When T_{ab} increased from 18°C to 24°C, $\dot{Q}_{gs}$ varied from 3,488 W to 4,586.8 W, increased by 24%, respectively. The variation trend was almost linear. $\dot{W}_{cp}$ increased with the increased of T_{ab}. When T_{ab} increased from 18°C to 24°C, $\dot{W}_{cp}$ varied from 971 W to 1,069.5 W, increased by 9.2%. COP_{chp} increased with the increased of T_{ab}. The reason of this phenomenon might be that the increasing degree of $\dot{Q}_{gs}$ was larger than that of $\dot{W}_{cp}$. When T_{ab} increased from 18°C to 24°C, COP_{chp} varied from 3.59 to 4.29, increased by 16.2%.

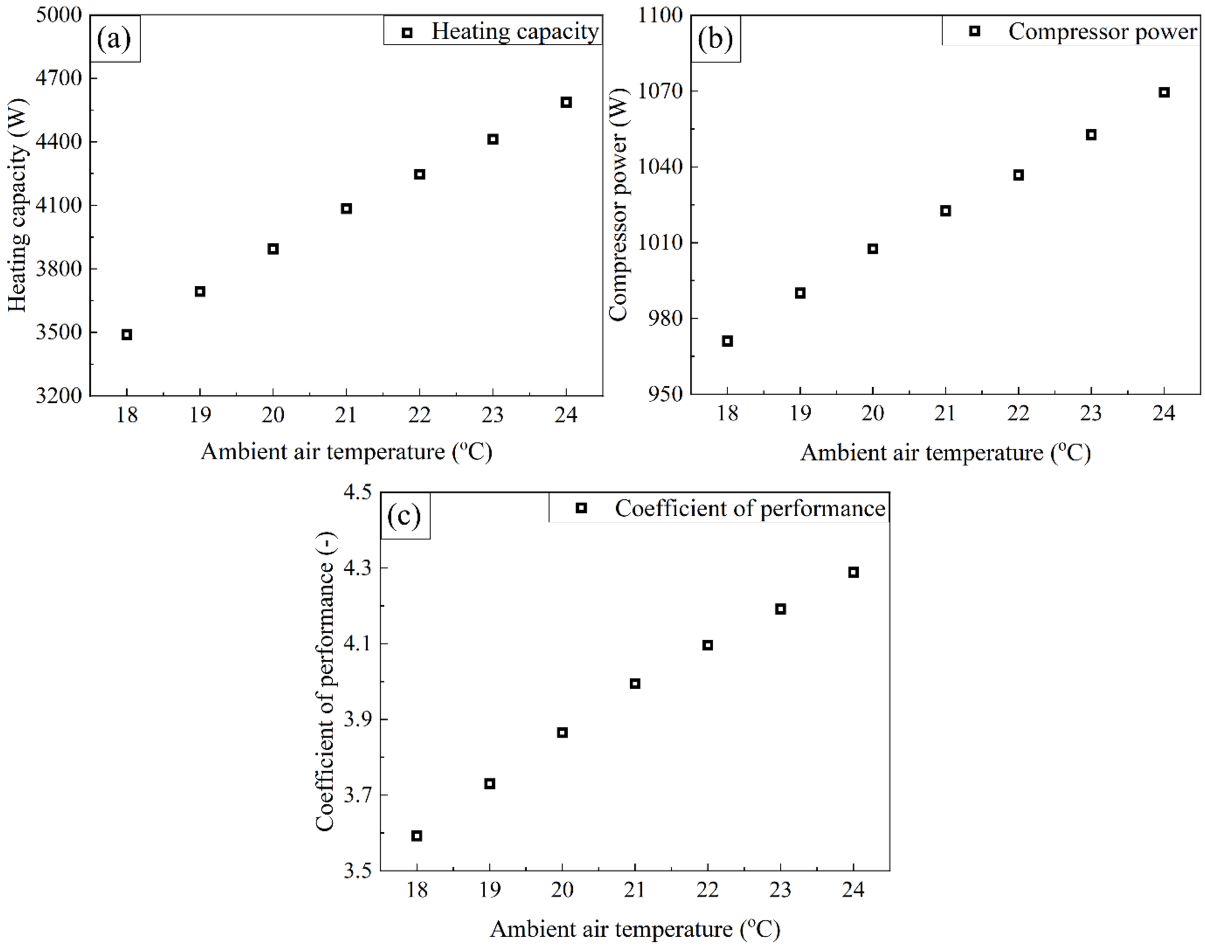

Fig. B1. Variations of (a) heating capacity, (b) compressor power, and (c) coefficient of performance with different ambient air temperature using the air-source heat pump

Fig. B2 (b) depicts the variations of $\dot{Q}_{gs}$, $\dot{W}_{cp}$, and COP_{chp} with different inlet mixture temperature in evaporator ($T_{it,z}$) using the water-source heat pump. $\dot{Q}_{gs}$ increased with the increase of $T_{it,z}$. The reason might be the enhancement of the heat transfer effect caused by the increasing temperature difference between the inlet mixture and CO_2 in the evaporator. When $T_{it,z}$ increased from 18°C to 24°C, $\dot{Q}_{gs}$ varied from 4,721.5 W to 7,075.8 W, increased by 49.9%, respectively. $\dot{W}_{cp}$ increased with the increased of $T_{it,z}$. When $T_{it,z}$ increased from 18°C to 24°C, $\dot{W}_{cp}$ varied from 1,082.5 W to 1,310 W, increased by 21%. COP_{chp} increased with the increased of $T_{it,z}$. This might be caused by that the increasing degree of $\dot{Q}_{gs}$ was larger than that of $\dot{W}_{cp}$. When $T_{it,z}$ increased from 18°C to 24°C, COP_{chp} varied from 4.36 to 5.4, increased by 23.8%.

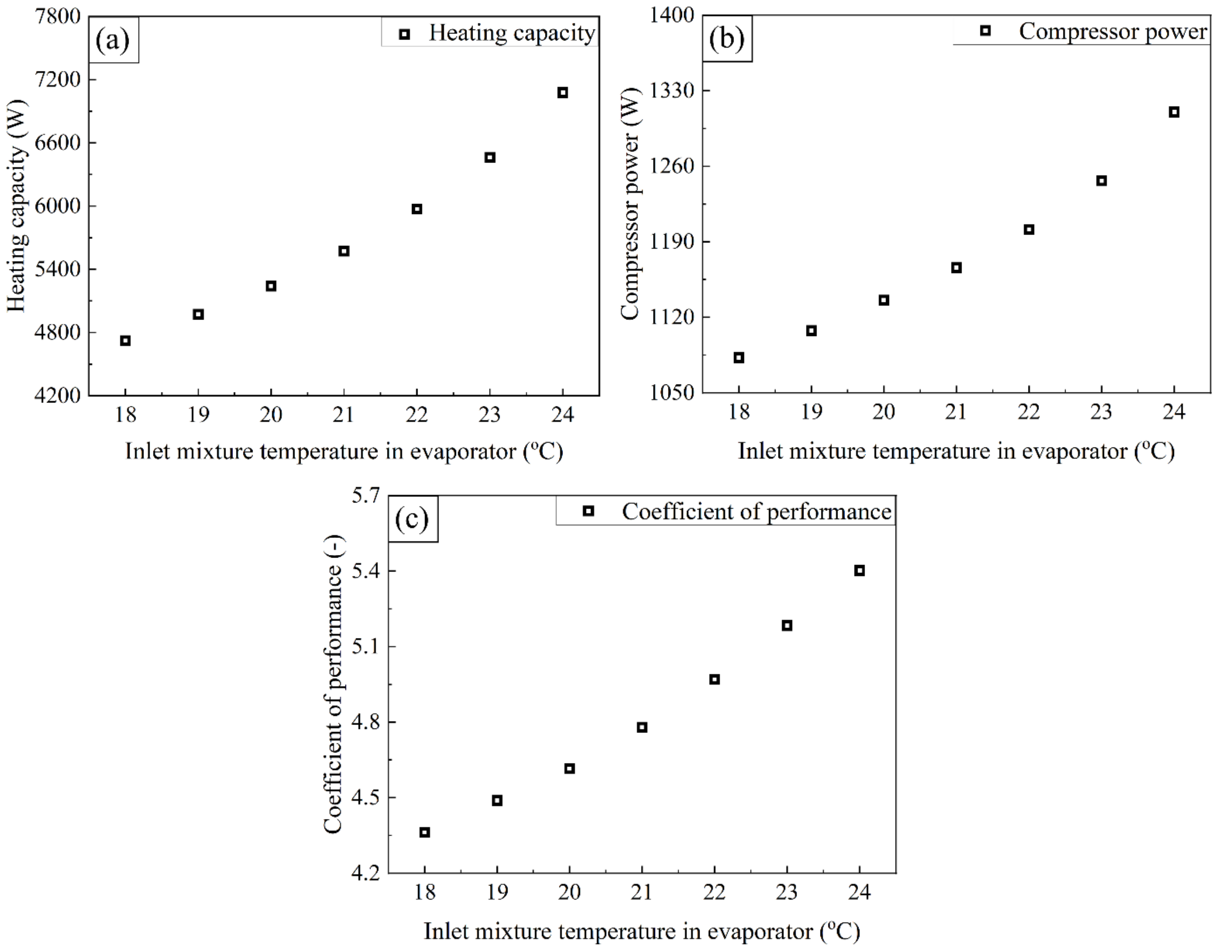

Fig. B2. Variations of (a) heating capacity, (b) compressor power, and (c) coefficient of performance with different inlet mixture temperature in evaporator using the water-source heat pump

Appendix C. Exergy analysis

The exergy efficiency of the PCM storage tank (η_{ey}) was calculated by Eqn. (C1):

$$\eta_{ey} = \frac{EX_{st}}{EX_{sd}} \tag{C1}$$

where EX_{st} and EX_{sd} denote the stored and supplied exergy by the water, respectively. The calculation of EX_{st} and EX_{sd} referred to the study of Cheng et al. [51]. EX_{st} was calculated by Eqn. (C2):

$$EX_{st} = EX_{wt} + EX_{pc} \tag{C2}$$

where EX_{wt} and EX_{pc} denote the exergy stored in the water and PCM, respectively. EX_{wt} was calculated by Eqn. (C3):

$$EX_{wt} = \sum_i M_{wt,i} c_{wt} \left(T_{ab} ln \frac{T_{in}}{T_{wt,i}} + T_{wt,i} - T_{in}\right) \tag{C3}$$

where M and c denote the mass and specific heat, respectively. EX_{pc} was calculated by Eqn. (C4):

$$EX_{pc} = \sum_i \int_{T_{in}}^{T} M_{pc,i}(\frac{T_{ab}}{T} - 1)dh(T) \quad \text{(C4)}$$

where h denotes the enthalpy. EX_{sd} was calculated by Eqn. (C5):

$$EX_{sd} = \int_0^t \dot{m}_{wt} c_{wt}(T_{ab} ln\frac{T_{wt,ot}}{T_{wt,it}} - T_{wt,ot} + T_{wt,it})\, dt \quad \text{(C5)}$$

Fig. C1 depicts the variations of exergy efficiency (η_{ey}) with different PCM types and tank arrangements using the air-source heat pump. When the PCM-1, PCM-2, PCM-3, PCM-4, PCM-5, and PCM-6 were used, η_{ey} were 14.2%, 15.9%, 18.7%, 31.8%, 22.7%, and 41.2%, respectively. Thus, η_{ey} was the minimum when the PCM-1 was utilized, while η_{ey} was the maximum when the PCM-6 was utilized. η_{ey} when the PCM-6 was utilized was 2.9 times as high as η_{ey} when the PCM-1 was utilized. η_{ey} in Case 1, Case 2, Case 3, Case 4, Case 5, and Case 6 were 38.2%, 36.3%, 33.3%, 32%, 31.7%, and 30.7%, respectively. Thus, η_{ey} in Case 6 had its minimum, while η_{ey} in Case 1 had its maximum. η_{ey} in Case 1 was 1.24 times as high as η_{ey} in Case 6. According to the Eqn. (C1), the variation of η_{ey} was determined by the variations of EX_{st} and EX_{pc}. When the increasing degree of EX_{st} was larger than that of EX_{pc}, η_{ey} would increase, and vice versa.

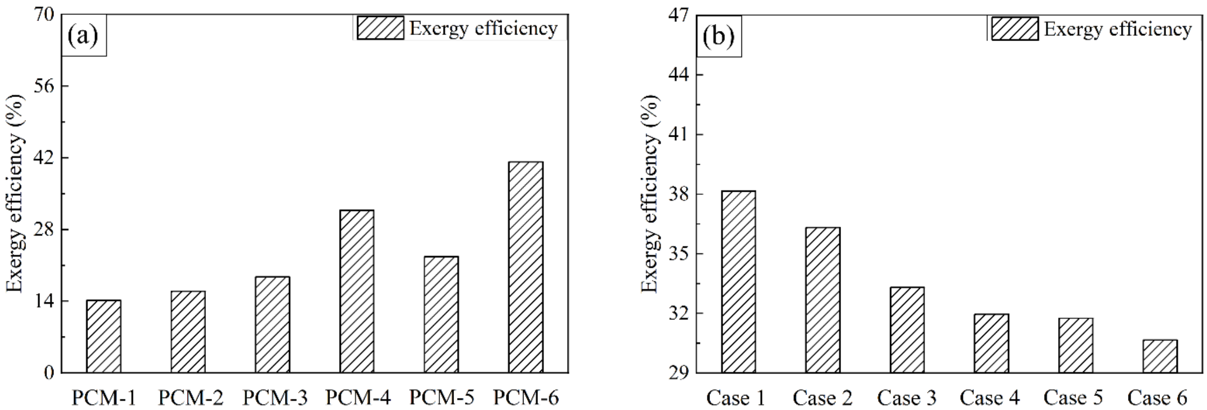

Fig. C1. Variations of exergy efficiency with different (a) PCM types and (b) tank arrangements using the air-source heat pump

Fig. C2 depicts the variations of exergy efficiency (η_{ey}) with different PCM types and tank arrangements using the water-source heat pump. When the PCM-1, PCM-2, PCM-3, PCM-4, PCM-5, and PCM-6 were used, η_{ey} were 31.3%, 14.6%, 38.2%, 55.7%, 24.3%, and 60.5%, respectively. Thus, η_{ey} was the minimum when the PCM-2 was utilized, while η_{ey} was the maximum when the PCM-6 was utilized. η_{ey} when the PCM-6 was utilized was 4.14 times as high as η_{ey} when the PCM-2 was utilized. η_{ey} in Case 1, Case 2, Case 3, Case 4, Case 5, and Case 6 were 55.1%, 55.1%, 55%, 55.8%, 55.7%, and 55.5%, respectively. Thus, η_{ey} in Case 3 had its minimum, while η_{ey} in Case 4 had its maximum. η_{ey} in Case 4 was 1.01 times as high as η_{ey} in Case 3. According to the Eqn. (C1), the relative increasing or decreasing degree of EX_{st} and EX_{pc} were the reason for the variations of η_{ey} in different PCM types and tank arrangements.

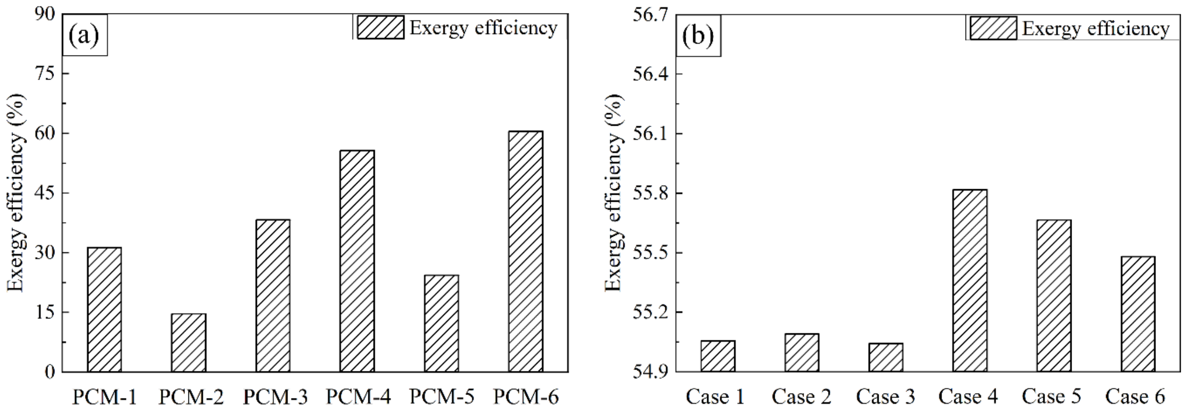

Fig. C2. Variations of exergy efficiency with different (a) PCM types and (b) tank arrangements using the water-source heat pump

References

[1] Z. Ding, W. Wu, A hybrid compression-assisted absorption thermal battery with high energy storage density/efficiency and low charging temperature, Applied Energy 282 (2021).

[2] Y. Du, B. Blocken, S. Pirker, A novel approach to simulate pollutant dispersion in the built environment: Transport-based recurrence CFD, Building and Environment 170 (2020).

[3] Y. Li, N. Nord, H. Wu, Z. Yu, G. Huang, A study on the integration of air-source heat pumps, solar collectors, and PCM tanks for outdoor swimming pools for winter application in subtropical climates, Journal of Building Performance Simulation 13(6) (2020) 662-683.

[4] Z. Wu, S. You, H. Zhang, Y. Wang, Y. Jiang, Z. Liu, L. Sha, S. Wei, Experimental investigations and multi-objective optimization of an air-source absorption heat pump for residential district heating, Energy Conversion and Management 240 (2021).

[5] S. Tangellapalli, Humidification-dehumidification and heat pump integration for water purifier and air conditioning, Energy Conversion and Management 244 (2021).

[6] J. Li, Z. Yang, H. Li, S. Hu, Y. Duan, J. Yan, Optimal schemes and benefits of recovering waste heat from data center for district heating by CO2 transcritical heat pumps, Energy Conversion and Management 245 (2021).

[7] F. Alshehri, S. Beck, D. Ingham, L. Ma, M. Pourkashanian, Sensitivity analysis of a vertical geothermal heat pump system in a hot dry climate, Renewable Energy 178 (2021) 785-801.

[8] M. Dongellini, C. Naldi, G.L. Morini, Influence of sizing strategy and control rules on the energy saving potential of heat pump hybrid systems in a residential building, Energy Conversion and Management 235 (2021).

[9] Y. Wang, Z. Quan, H. Jing, L. Wang, Y. Zhao, Performance and operation strategy optimization of a new dual-source building energy supply system with heat pumps and energy storage, Energy Conversion and Management 239 (2021).

[10] J. Vivian, E. Prataviera, F. Cunsolo, M. Pau, Demand Side Management of a pool of air source heat pumps for space heating and domestic hot water production in a residential district, Energy Conversion and Management 225 (2020).

[11] G. Kosmadakis, C. Arpagaus, P. Neofytou, S. Bertsch, Techno-economic analysis of high-temperature heat pumps with low-global warming potential refrigerants for upgrading waste heat up to 150 °C, Energy Conversion and Management 226 (2020).

[12] Y.-M. Li, C.-C. Wang, Investigation of the performance of a transcritical CO2 heat pump system subject to heated water conditions: Perspective from the second law, Applied Thermal Engineering 193 (2021).

[13] B. Dai, H. Qi, W. Dou, S. Liu, D. Zhong, H. Yang, V. Nian, Y. Hao, Life cycle energy, emissions and cost evaluation of CO2 air source heat pump system to replace traditional heating methods for residential heating in China: System configurations, Energy Conversion and Management 218 (2020).

[14] H. Ghazizade-Ahsaee, I. Baniasad Askari, The application of thermoelectric and ejector in a CO2 direct-expansion ground source heat pump; energy and exergy analysis, Energy Conversion and Management 226 (2020).

[15] J. Wang, M. Belusko, M. Liu, H. Semsarilar, R. Liddle, A. Alemu, M. Evans, C. Zhao, J. Hudson, F. Bruno, A comprehensive study on a novel transcritical CO2 heat pump for simultaneous space heating and cooling – Concepts and initial performance, Energy Conversion and Management 243 (2021).

[16] H.J. Chung, C. Baek, H. Kang, D. Kim, Y. Kim, Performance evaluation of a gas injection CO2 heat pump according to operating parameters in extreme heating and cooling conditions, Energy 154 (2018) 337-345.

[17] Y. Li, N. Nord, N. Zhang, C. Zhou, An ANN-based optimization approach of building energy systems: Case study of swimming pool, Journal of Cleaner Production 277 (2020).

[18] E. Oró, A. de Gracia, A. Castell, M.M. Farid, L.F. Cabeza, Review on phase change materials (PCMs) for cold thermal energy storage applications, Applied Energy 99 (2012) 513-533.

[19] X. Hu, X. Gong, F. Zhu, X. Xing, Z. Li, X. Zhang, Thermal analysis and optimization of metal foam PCM-based heat sink for thermal management of electronic devices, Renewable Energy 212 (2023) 227-237.

[20] Y. Gao, Z. Dai, D. Wu, C. Wang, B. Chen, X. Zhang, Transient performance assessment of a hybrid PV-TEG system integrated with PCM under non-uniform radiation conditions: A numerical investigation, Renewable Energy 198 (2022) 352-366.

[21] C. Piselli, M. Prabhakar, A. de Gracia, M. Saffari, A.L. Pisello, L.F. Cabeza, Optimal control of natural ventilation as passive cooling strategy for improving the energy performance of building envelope with PCM integration, Renewable Energy 162 (2020) 171-181.

[22] A. Egea, A. García, R. Herrero-Martín, J. Pérez-García, Experimental performance of a novel scraped surface heat exchanger for latent energy storage for domestic hot water generation, Renewable Energy 193 (2022) 870-878.

[23] A.H. Mosaffa, L. Garousi Farshi, C.A. Infante Ferreira, M.A. Rosen, Energy and exergy evaluation of a multiple-PCM thermal storage unit for free cooling applications, Renewable Energy 68 (2014) 452-458.

[24] M. Carmona, A. Rincón, L. Gulfo, Energy and exergy model with parametric study of a hot water storage tank with PCM for domestic applications and experimental validation for multiple operational scenarios, Energy Conversion and Management 222 (2020).

[25] O.G. Pop, M.C. Balan, A numerical analysis on the performance of DHW storage tanks with immersed PCM cylinders, Applied Thermal Engineering 197 (2021).

[26] R. Koželj, U. Mlakar, E. Zavrl, U. Stritih, R. Stropnik, An experimental and numerical analysis of an improved thermal storage tank with encapsulated PCM for use in retrofitted buildings for heating, Energy and Buildings 248 (2021).

[27] H. Huang, Y. Xiao, J. Lin, T. Zhou, Y. Liu, Q. Zhao, Improvement of the efficiency of solar thermal energy storage systems by cascading a PCM unit with a water tank, Journal of Cleaner Production 245 (2020).

[28] C. Zhao, M. Opolot, M. Liu, F. Bruno, S. Mancin, K. Hooman, Phase change behaviour study of PCM tanks partially filled with graphite foam, Applied Thermal Engineering 196 (2021).

[29] X.-Y. Li, L. Yang, X.-L. Wang, X.-Y. Miao, Y. Yao, Q.-Q. Qiang, Investigation on the charging process of a multi-PCM latent heat thermal energy storage unit for use in conventional air-conditioning systems, Energy 150 (2018) 591-600.

[30] M. Gorzin, M.J. Hosseini, A.A. Ranjbar, R. Bahrampoury, Investigation of PCM charging for the energy saving of domestic hot water system, Applied Thermal Engineering 137 (2018) 659-668.

[31] A. Alhusseny, N. Al-Zurfi, A. Nasser, A. Al-Fatlawi, M. Aljanabi, Impact of using a PCM-metal foam composite on charging/discharging process of bundled-tube LHTES units, International Journal of Heat and Mass Transfer 150 (2020).

[32] G.S. Sodhi, P. Muthukumar, Compound charging and discharging enhancement in multi-PCM system using non-uniform fin distribution, Renewable Energy 171 (2021) 299-314.

[33] B.P. Rasmussen, A.G. Alleyne, Dynamic modeling and advanced control of air conditioning and refrigeration systems, Air Conditioning and Refrigeration Center. College of Engineering …, 2006.

[34] W. Deng, J. Yu, Simulation analysis on dynamic performance of a combined solar/air dual source heat pump water heater, Energy Conversion and Management 120 (2016) 378-387.

[35] F.A. Mota, E. Carvalho, M.A. Ravagnani, Modeling and Design of Plate Heat Exchanger, Heat Transfer: Studies and Applications (2015) 165.

[36] E. Lee, H. Kang, Y. Kim, Flow boiling heat transfer and pressure drop of water in a plate heat exchanger with corrugated channels at low mass flux conditions, International Journal of Heat and Mass Transfer 77 (2014) 37-45.

[37] S. Wang, H. Tuo, F. Cao, Z. Xing, Experimental investigation on air-source transcritical CO2 heat pump water heater system at a fixed water inlet temperature, International Journal of Refrigeration 36(3) (2013) 701-716.

[38] Y. Li, N. Nord, H. Halvorsen, I.H. Rekstad, Model-based sizing of a CO2 heat pump for residential use, Sustainable Energy Technologies and Assessments 53 (2022) 102592.

[39] I.W. Eames, A. Milazzo, G.G. Maidment, Modelling thermostatic expansion valves, International Journal of Refrigeration 38 (2014) 189-197.

[40] Y. Li, G. Huang, H. Wu, T. Xu, Feasibility study of a PCM storage tank integrated heating system for outdoor swimming pools during the winter season, Applied Thermal Engineering 134 (2018) 490-500.

[41] Y. Li, G. Huang, T. Xu, X. Liu, H. Wu, Optimal design of PCM thermal storage tank and its application for winter available open-air swimming pool, Applied Energy 209 (2018) 224-235.

[42] T. Watanabe, H. Kikuchi, A. Kanzawa, Enhancement of charging and discharging rates in a latent heat storage system by use of PCM with different melting temperatures, Heat Recovery Systems and CHP 13(1) (1993) 57-66.

[43] Y. Li, N. Nord, I.H. Rekstad, S.K. Skånøy, L.K. Sørensen, Study of a water-source CO2 heat pump for residential use: experimental discharge pressure control and performance analysis, E3S Web of Conferences, EDP Sciences, 2021, p. 06010.

[44] H. Wan, X. Xu, A. Li, T. Yan, W. Gang, A wet-bulb temperature-based control method for controlling the heat balance of the ground soil of a hybrid ground-source heat pump system, Advances in Mechanical Engineering 9(6) (2017).

[45] W. Youssef, Y.T. Ge, S.A. Tassou, CFD modelling development and experimental validation of a phase change material (PCM) heat exchanger with spiral-wired tubes, Energy Conversion and Management 157 (2018) 498-510.

[46] Phase Change Products Pty Ltd, Thermal Properties of PC17. https://pcpaustralia.com.au/pcm-range-products/pc17/.

[47] M. Koschenz, B. Lehmann, Development of a thermally activated ceiling panel with PCM for application in lightweight and retrofitted buildings, Energy and Buildings 36(6) (2004) 567-578.

[48] C. Arkar, S. Medved, Optimization of latent heat storage in solar air heating system with vacuum tube air solar collector, Solar Energy 111 (2015) 10-20.

[49] D. Qi, L. Pu, F. Sun, Y. Li, Numerical investigation on thermal performance of ground heat exchangers using phase change materials as grout for ground source heat pump system, Applied Thermal Engineering 106 (2016) 1023-1032.

[50] Y. Berthou, P.H. Biwole, P. Achard, H. Sallée, M. Tantot-Neirac, F. Jay, Full scale experimentation on a new translucent passive solar wall combining silica aerogels and phase change materials, Solar Energy 115 (2015) 733-742.

[51] X. Cheng, X. Zhai, R. Wang, Thermal performance analysis of a packed bed cold storage unit using composite PCM capsules for high temperature solar cooling application, Applied Thermal Engineering 100 (2016) 247-255.